Isospin decomposition of $\gamma N \to N^*$ transitions within a dynamical coupled-channels model

H. Kamano,[1,2,*] S. X. Nakamura,[3] T.-S. H. Lee,[4] and T. Sato[3]

[1]*KEK Theory Center, Institute of Particle and Nuclear Studies (IPNS), High Energy Accelerator Research Organization (KEK), Tsukuba, Ibaraki 305-0801, Japan*

[2]*J-PARC Branch, KEK Theory Center, IPNS, KEK, Tokai, Ibaraki 319-1106, Japan*

[3]*Department of Physics, Osaka University, Toyonaka, Osaka 560-0043, Japan*

[4]*Physics Division, Argonne National Laboratory, Argonne, Illinois 60439, USA*

(Received 2 May 2016; published 7 July 2016)

By extending the dynamical coupled-channels analysis performed in our previous work [Phys. Rev. C **88**, 035209 (2013)] to include the available data of photoproduction of π mesons off neutrons, the transition amplitudes for the photoexcitation of the neutron-to-nucleon resonances, $\gamma n \to N^*$, at the resonance pole positions are determined. The combined fits to the data for both the proton- and neutron-target reactions also revise our results for the resonance pole positions and the $\gamma p \to N^*$ transition amplitudes. Our results allow an isospin decomposition of the $\gamma N \to N^*$ transition amplitudes for the isospin $I = \frac{1}{2}$ N^* resonances, which is necessary for testing hadron structure models and gives crucial inputs for constructing models of neutrino-induced reactions in the nucleon resonance region.

DOI: 10.1103/PhysRevC.94.015201

I. INTRODUCTION

Extracting the parameters, such as masses, widths, and form factors, associated with the N and Δ resonances (collectively referred to as N^*) from the data of meson-production reactions is an important task for understanding quantum chromodynamics (QCD) in the nonperturbative domain. It is usually done by performing a comprehensive partial-wave analysis of πN and γN reactions with various final states including πN, $\pi\pi N$, ηN, $K\Lambda$, $K\Sigma$, ωN, etc. within the on-shell K-matrix approaches [1–4] and the dynamical-model approaches [5–7]. Here, the unitarity is a key essential element in accomplishing such a comprehensive analysis and making a reliable extraction of resonance parameters, because it not only ensures the conservation of probability in multichannel reaction processes but also properly defines the analytic structure of the scattering amplitudes in the complex-energy plane. The latter is crucial for correctly extracting from the data the resonance parameters defined at the poles of scattering amplitudes.

Among the N^* resonance parameters, transition amplitudes for the photo- and electro-excitation of the nucleon to N^* resonances, $\gamma^{(*)}N \to N^*$, have been a particular focus of interest in the N^* spectroscopy because of its crucial role in understanding the electromagnetic properties as well as the quark-gluon substructure of N^* resonances (see, e.g., Ref. [8]). In fact, the dynamical-model studies [9–12] of photon- and electron-induced meson-production reactions off the proton target revealed the large meson-cloud effect on the transition amplitudes at low Q^2 whereas it decreases when Q^2 is increased, implying that the (constituent) quark-gluon core of N^* surrounded by dense meson clouds at long-distance scales gradually emerges at shorter-distance scales. In this regard, new extensive measurements of $ep \to e'X$ with $X = \pi N, \pi\pi N, KY$ are planned at CLAS12 [13], aiming at precise determinations of the $\gamma^{(*)}p \to N^*$ transition amplitudes in the Q^2 region where such a transition to the "core-dominated" region is expected to occur.

However, for the $I = \frac{1}{2}$ N^* resonances, the $\gamma^{(*)}N \to N^*$ transition amplitudes for both the proton ($N = p$) and neutron ($N = n$) are necessary to uniquely determine the isospin structure of the photo- and electro-excitation couplings. The information on such isospin-decomposed transition amplitudes are also important for investigating the neutrino-induced reactions in the N^* resonance region (see, e.g., Ref. [14]) because those are the basic ingredients for constructing the vector-current matrix elements associated with the weak interactions. The analysis of the photo- and electro-production reactions on both the proton and neutron targets is required to determine the isospin structure of the $\gamma^{(*)}N \to N^*$ transition amplitudes for the $I = \frac{1}{2}$ N^* resonances,[1] and such combined analyses have been done so far by several analysis groups [15,16] within the coupled-channels framework.

In Ref. [5], we reported on the N^* parameters extracted within the dynamical coupled-channels (DCC) model developed in Ref. [17]. Our approach is to fit the meson production data and to also search for the resonance poles by solving the following coupled integral equations for the partial-wave amplitudes, $T_{\beta,\alpha}(p_\beta, p_\alpha; W)$, which are specified by the total angular momentum J, parity P, and total isospin I (these

*kamano@post.kek.jp

[1]For the $I = \frac{3}{2}$ N^* resonances, the $\gamma^{(*)}p \to N^*$ and $\gamma^{(*)}n \to N^*$ transition amplitudes are the same, and thus in principle only the data for either the proton- or neutron-target reaction is required. However, it is still highly desirable to have the data for both reactions so that one can have more constraints on the transition amplitudes for $I = \frac{3}{2}$ N^* resonances as well.

indices are suppressed in the following equations):

$$T_{\beta,\alpha}(p_\beta,p_\alpha;W) = V_{\beta,\alpha}(p_\beta,p_\alpha;W) + \sum_\delta \int p^2 dp \times V_{\beta,\delta}(p_\beta,p;W) G_\delta(p;W) \times T_{\delta,\alpha}(p,p_\alpha;W), \quad (1)$$

with

$$V_{\beta,\alpha}(p_\beta,p_\alpha;W) = v_{\beta,\alpha}(p_\beta,p_\alpha) + Z_{\beta,\alpha}(p_\beta,p_\alpha;W) + \sum_{N_n^*} \frac{\Gamma_{\beta,N_n^*}(p_\beta)\Gamma_{N_n^*,\alpha}(p_\alpha)}{W - M^0_{N_n^*}}. \quad (2)$$

Here, the subscripts $\alpha,\beta,\delta = \pi N, \eta N, K\Lambda, K\Sigma, \pi\Delta, \rho N, \sigma N$ represent reaction channels considered, for which the $\pi\Delta$, ρN, and σN channels are the resonant components of the three-body $\pi\pi N$ channel. (Indices for the orbital angular momentum L and total spin S of each reaction channel are suppressed.) $G_\delta(p,W)$ is the Green's function of channel δ; $M^0_{N_n^*}$ is the mass of the nth bare excited nucleon state N_n^* in a given partial wave; the hadron-exchange potential $v_{\beta,\alpha}$ is derived from the effective Lagrangians by making use of the unitary transformation method[2] [18,19]; the energy-dependent $Z_{\beta,\alpha}(p_\beta,p_\alpha;W)$ term [17] is the effective one-particle-exchange potential that is derived with the projection operator method [20] and produces the three-body $\pi\pi N$ cut; the vertex interaction Γ_{α,N_n^*} defines the $N_n^* \to \alpha$ decay (note $\Gamma_{\alpha,N_n^*} = \Gamma^\dagger_{N_n^*,\alpha}$). A similar approach is also taken in Ref. [6]. The differences between our approach and the other coupled-channels analyses [2–4], which only consider the on-shell matrix elements of $T_{\alpha,\beta}(p_\alpha,p_\beta;W)$, have been discussed in detail in Refs. [5,17,21]. Here we only mention that these models can be qualitatively obtained from Eq. (1) by keeping only the on-shell part of the propagator $G_\delta(p;W)$, and Refs. [2,4] further replace the hadron-exchange interaction $V_{\beta,\alpha}$ by phenomenological forms such as the polynomials of on-shell momenta. If the data are *complete* (as explained, e.g., in Ref. [22]) and high-accuracy fits can be achieved, all approaches are acceptable for extracting the resonance pole positions. However, more investigations are needed to examine under what ideal conditions all approaches should give the same resonance parameters defined at the poles of the scattering amplitudes. Furthermore, it is practically impossible to get *complete* data. Thus it is essential to impose theoretical constraints on both the determinations of the partial-wave amplitudes and the extractions of N^* parameters. This is accomplished in our approach by implementing the well-established hadron-exchange mechanisms, as defined by $v_{\beta,\alpha}$ in Eq. (2), in the fits. This also allows us to provide interpretations of the structure of the extracted N^* resonances, such as the meson-cloud effects on the $\gamma^{(*)}N \to N^*$ transitions.

[2]The potential derived with the unitary transformation method becomes energy independent. The off-shell behavior of the potential is also defined within this method.

For the calculations of the γN reaction amplitudes, we use the so-called helicity-LSJ mixed representation [17], in which the initial γN state is specified by their helicities, λ_γ and λ_N, while the final meson-baryon state is specified by L, S, J, and I as in Eq. (1),

$$T_{\beta,\gamma N(\lambda)}(p_\beta,q;W) = V_{\beta,\gamma N(\lambda)}(p_\beta,q;W) + \sum_\delta \int p^2 dp \times T_{\beta,\delta}(p_\beta,p;W) G_\delta(p;W) \times V_{\delta,\gamma N(\lambda)}(p,q;W), \quad (3)$$

$$V_{\beta,\gamma N(\lambda)}(p_\beta,q;W) = v_{\beta,\gamma N(\lambda)}(p_\beta,q) + \sum_{N_n^*} \frac{\Gamma_{\beta,N_n^*}(p_\beta)\Gamma_{N_n^*,\gamma N(\lambda)}(q)}{W - M^0_{N_n^*}}, \quad (4)$$

where $\lambda = \lambda_\gamma - \lambda_N$. Here we note that the summation in Eq. (3) runs over only hadronic meson-baryon channels. We take γN channel perturbatively since the electromagnetic interactions are much smaller than the strong ones and their effect on the resonance parameters are expected to be just the order of isospin breaking. The potential $v_{\beta,\gamma N(\lambda)}(p_\beta,q)$ is again derived from the effective Lagrangians by making use of the unitary transformation method. On the other hand, in Ref. [6] the potential for electromagnetic interaction is simply parametrized with polynomials.

In our previous work [5], we analyzed the available data of πp, $\gamma p \to \pi N$, ηN, $K\Lambda$, $K\Sigma$ reactions in the region of $W \lesssim 2.1$ GeV. Then 24 physical N^* resonances, which are defined at the poles of the scattering amplitudes in the complex energy plane, were successfully extracted. Their properties, including the $\gamma p \to N^*$ transition amplitudes, were also extracted by evaluating the residues of the scattering amplitudes at the resonance poles.

As a first step towards understanding the isospin structure of the photo- and electro-excitation of the nucleon to the $I = \frac{1}{2}$ N^* resonances, in this work we extend our previous DCC analysis [5] by further including the data available for π photoproductions off the neutron and making a combined analysis of meson production reactions off the proton and neutron targets. We then present the extracted $\gamma n \to N^*$ transition amplitudes, together with the improved results for resonance pole masses, πN elastic residues, and the $\gamma p \to N^*$ transition amplitudes. In this work, we focus on studying the transition amplitudes at the photon point, $Q^2 = 0$.

Our procedures of resonance extraction have been given in detail in Refs. [5,12,23–25]. We therefore will only recall in Sec. II the formulas that are needed for presenting the parameters of the extracted $\gamma N \to N^*$ transitions. In Sec. III, we present our fits to the data. The extracted $\gamma n \to N^*$ transition amplitudes are presented in Sec. IV, along with the revised values of resonance pole positions and the $\gamma p \to N^*$ transition amplitudes presented in Ref. [5]. In Sec. V, we give a summary and discuss the necessary future works.

II. FORMULAS FOR $\gamma N \to N^*$ TRANSITION AMPLITUDES

To define the $\gamma N \to N^*$ transition amplitudes, we recall here some formula that can be derived [5,17,25] from Eqs. (1) and (3) within the dynamical coupled-channels model considered. The on-shell S-matrix elements of the meson-baryon reactions, $MB \to M'B'$, in the center-of-mass system are given for each partial wave by

$$S_{M'B',MB}(W) = \delta_{M'B',MB} + 2i\,F_{M'B',MB}(W). \tag{5}$$

Here W is the total scattering energy and we have suppressed indices for the angular momenta, parity, and isospin quantum numbers associated with the channels MB and $M'B'$. The on-shell scattering amplitudes $F_{M'B',MB}(W)$ are related to the T-matrix elements given by Eq. (1) as follows:

$$\begin{aligned} F_{M'B',MB}(W) = &-\left[\rho_{M'B'}\left(k^{\rm on}_{M'B'};W\right)\right]^{1/2} \\ &\times T_{M'B',MB}\left(k^{\rm on}_{M'B'},k^{\rm on}_{MB};W\right) \\ &\times \left[\rho_{MB}\left(k^{\rm on}_{MB};W\right)\right]^{1/2}, \end{aligned} \tag{6}$$

with

$$\rho_{MB}(k_{MB};W) = \pi\frac{k_{MB}E_M(k_{MB})E_B(k_{MB})}{W}, \tag{7}$$

where $E_\alpha(k_\alpha) = (m_\alpha^2 + k_\alpha^2)^{1/2}$ is the energy of a particle α with mass m_α and three-momentum $\vec{k}_\alpha$ ($k_\alpha \equiv |\vec{k}_\alpha|$). For a given W, which can be complex, the on-shell momentum for the channel MB, $k^{\rm on}_{MB}$, is defined by $W = E_M(k^{\rm on}_{MB}) + E_B(k^{\rm on}_{MB})$.

As the energy W approaches a pole position M_R in the complex W plane, the scattering amplitudes take the form

$$F_{M'B',MB}(W \to M_R) = -\frac{R_{M'B',MB}}{W - M_R} + B_{M'B',MB}, \tag{8}$$

where $R_{M'B',MB}$ is the residue of $F_{M'B',MB}(W)$ at the resonance pole M_R and $B_{M'B',MB}$ is the "background" contribution. Both $R_{M'B',MB}$ and $B_{M'B',MB}$ are constant and in general complex. The pole position M_R and the residue $R_{M'B',MB}$ are fundamental quantities that characterize the extracted resonance.

The residues $R_{M'B',MB}$ defined in Eq. (8) can be calculated by using the definition

$$R_{M'B',MB} = \frac{1}{2\pi i}\oint_{C_{M_R}} dW[-F_{M'B',MB}(W)], \tag{9}$$

where C_{M_R} is an appropriate closed path in the neighborhood of the point $W = M_R$, circling $W = M_R$ in a counterclockwise manner. It can be shown that for partial waves with one or more bare states (this is the case of our current model for all partial waves), $R_{M'B',MB}$ can also be calculated [5,12,23] with

$$\begin{aligned} R_{M'B',MB} = &\left[\rho_{M'B'}\left(k^{\rm on}_{M'B'};M_R\right)\right]^{1/2}\bar{\Gamma}^R_{M'B'}\left(k^{\rm on}_{M'B'};M_R\right) \\ &\times \bar{\Gamma}^R_{MB}\left(k^{\rm on}_{MB};M_R\right)\left[\rho_{MB}\left(k^{\rm on}_{MB};M_R\right)\right]^{1/2}. \end{aligned} \tag{10}$$

Here, $\bar{\Gamma}^R_{MB}(k^{\rm on}_{MB};M_R)$ is the (renormalized) dressed $MB \to N^*$ vertex that contains the meson cloud arising from the coupling to the meson-baryon continuum states.

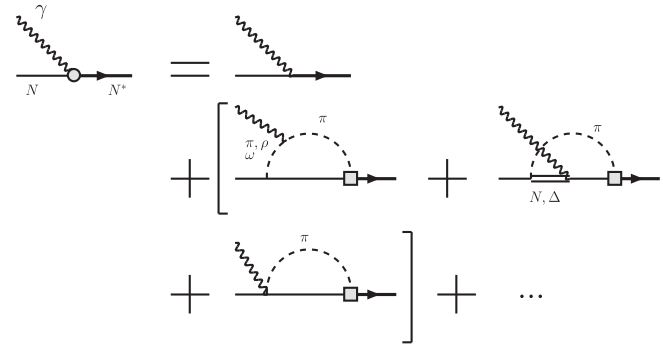

FIG. 1. Graphical representation of dressed $\gamma N \to N^*$ transition vertex.

As for the $\gamma N \to M'B'$ reactions, the on-shell scattering amplitudes are given in the helicity-LSJ mixed representation by

$$\begin{aligned} F_{M'B',\gamma N(\lambda)}(W) = &-\left[\rho_{M'B'}\left(k^{\rm on}_{M'B'};W\right)\right]^{1/2} \\ &\times T_{M'B',\gamma N(\lambda)}\left(k^{\rm on}_{M'B'},k^{\rm on}_{\gamma N};W\right) \\ &\times \left[\rho_{\gamma N}\left(k^{\rm on}_{\gamma N};W\right)\right]^{1/2}, \end{aligned} \tag{11}$$

where $k^{\rm on}_{\gamma N}$ is given by $W = k^{\rm on}_{\gamma N} + E_N(k^{\rm on}_{\gamma N})$. The amplitude $F_{M'B',\gamma N(\lambda)}(W)$ also has a form close to the resonance pole position M_R,

$$F_{M'B',\gamma N(\lambda)}(W \to M_R) = -\frac{R_{M'B',\gamma N(\lambda)}}{W - M_R} + B_{M'B',\gamma N(\lambda)}. \tag{12}$$

Then, the residue at the resonance pole M_R, $R_{M'B',\gamma N(\lambda)}$, can be calculated by using the same formula (9) as the $MB \to M'B'$ cases, or can be calculated by using the following formula similar to Eq. (10):

$$\begin{aligned} R_{M'B',\gamma N(\lambda)} = &\left[\rho_{M'B'}\left(k^{\rm on}_{M'B'};M_R\right)\right]^{1/2}\bar{\Gamma}^R_{M'B'}\left(k^{\rm on}_{M'B'};M_R\right) \\ &\times \bar{\Gamma}^R_{\gamma N(\lambda)}\left(k^{\rm on}_{\gamma N};M_R\right)\left[\rho_{\gamma N}\left(k^{\rm on}_{\gamma N};M_R\right)\right]^{1/2}, \end{aligned} \tag{13}$$

where the quantity $\bar{\Gamma}^R_{\gamma N(\lambda)}(k^{\rm on}_{\gamma N};M_R)$ is the dressed $\gamma N \to N^*$ vertex, as illustrated in Fig. 1, multiplied by an appropriate wave-function renormalization factor. The details on how to compute $\bar{\Gamma}^R_{MB}(k^{\rm on}_{MB};M_R)$ and $\bar{\Gamma}^R_{\gamma N(\lambda)}(k^{\rm on}_{\gamma N};M_R)$ etc. are given in Refs. [5,12,23].

With the renormalized vertex $\bar{\Gamma}^R_{\gamma N(\lambda)}(k^{\rm on}_{\gamma N};M_R)$, the helicity amplitudes for the $\gamma N \to N^*$ transitions evaluated at the

TABLE I. Observables and number of data points considered in this coupled-channels analysis. The data are taken from the database of the INS DAC Services [27].

Reactions	Observables	Number of data points
γ'n' $\to \pi^- p$	$d\sigma/d\Omega$	2305
	Σ	308
	T	94
	P	88
γ'n' $\to \pi^0 n$	$d\sigma/d\Omega$	148
	Σ	216

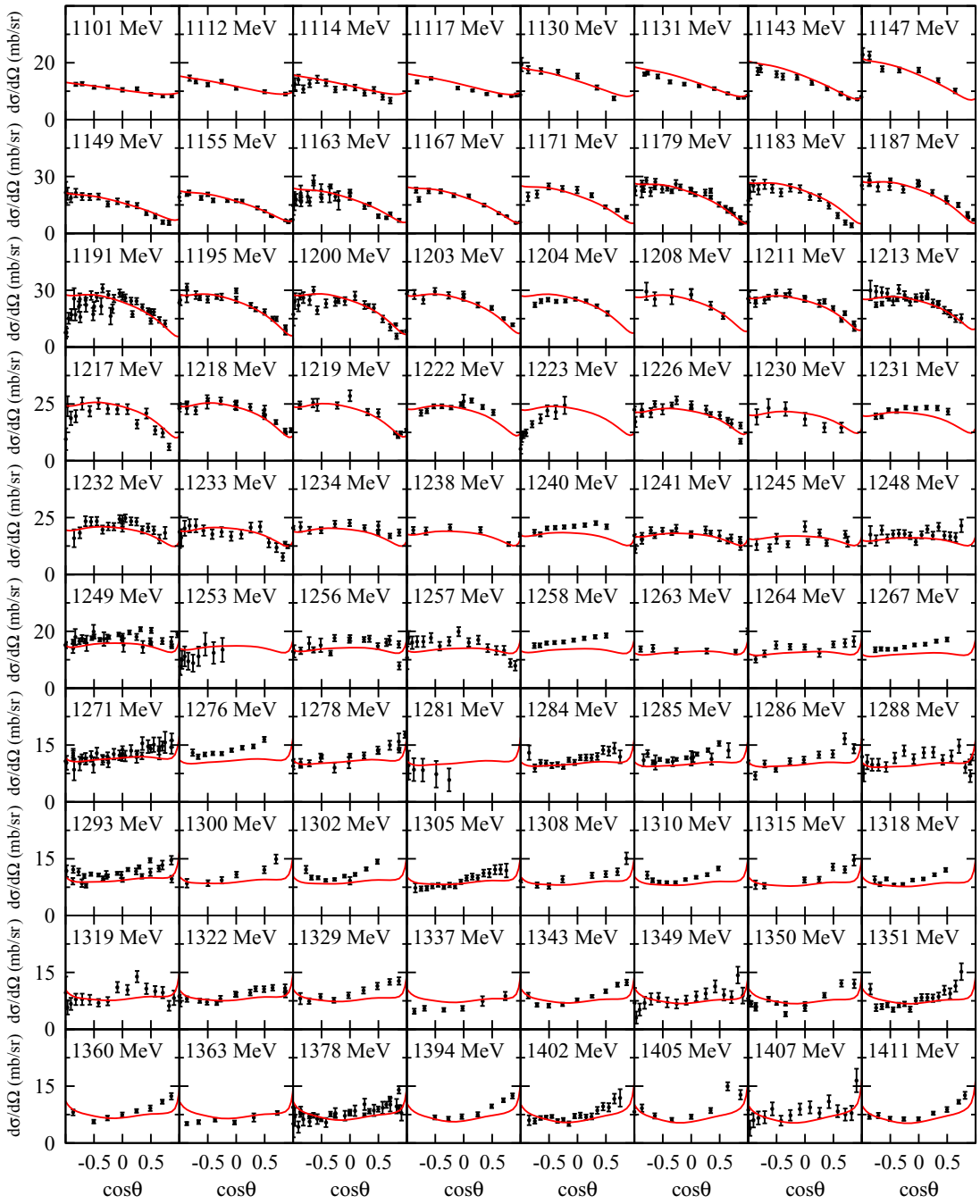

FIG. 2. Result of fit for $d\sigma/d\Omega$ of $\gamma\,'n' \to \pi^- p$.

resonance pole position M_R, $A_{3/2}$, and $A_{1/2}$, can be written as [12]

$$A_{3/2} = C\bar{\Gamma}^R_{\gamma N(3/2)}\left(k^{\rm on}_{\gamma N}; M_R\right), \tag{14}$$

$$A_{1/2} = C\bar{\Gamma}^R_{\gamma N(1/2)}\left(k^{\rm on}_{\gamma N}; M_R\right), \tag{15}$$

with

$$C = \sqrt{\frac{E_N\left(k^{\rm on}_{\gamma N}\right)}{m_N}}\frac{1}{\sqrt{2K}}\sqrt{\frac{(2J^R+1)(2\pi)^3 2\left|k^{\rm on}_{\gamma N}\right|}{4\pi}}, \tag{16}$$

where J^R is the spin of the resonance state and $K = (M_R^2 - m_N^2)/(2M_R)$.

By fitting to the data, the model parameters included in the potentials (2) and (4) are determined. We then can compute the on-shell dressed $\gamma N \to N^*$ vertices at the resonance pole position $\bar{\Gamma}^R_{\gamma N(\lambda)}(k^{\rm on}_{\gamma N}; M_R)$ and determine the helicity amplitudes A_λ by using Eqs. (14)–(16). In practice, however, we use an alternative formula from Ref. [26] to calculate the helicity amplitudes and unambiguously fix their phases. The formula is given with the residues $R_{\pi N,\gamma N(\lambda)}$ and $R_{\pi N,\pi N}$ as follows:

$$A_{3/2} = N R_{\pi N \gamma N(3/2)}, \tag{17}$$

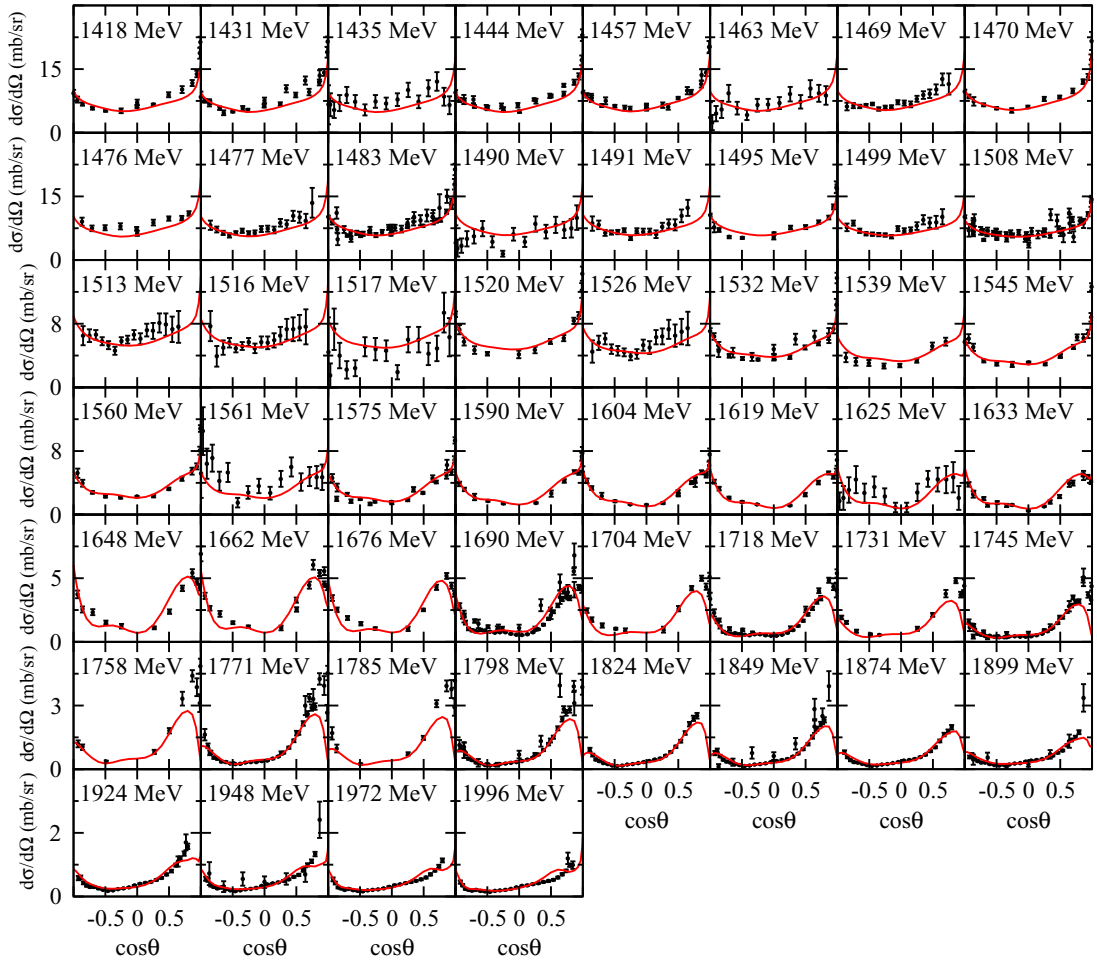

FIG. 3. Result of fit for $d\sigma/d\Omega$ of γ 'n' $\rightarrow \pi^- p$ (continued).

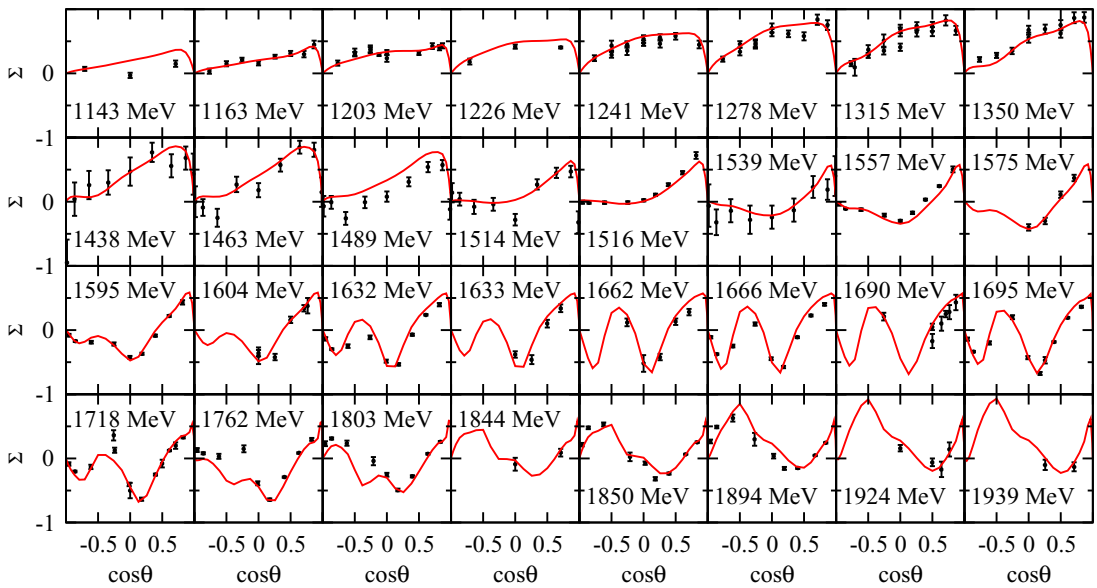

FIG. 4. Result of fit for Σ of γ 'n' $\rightarrow \pi^- p$.

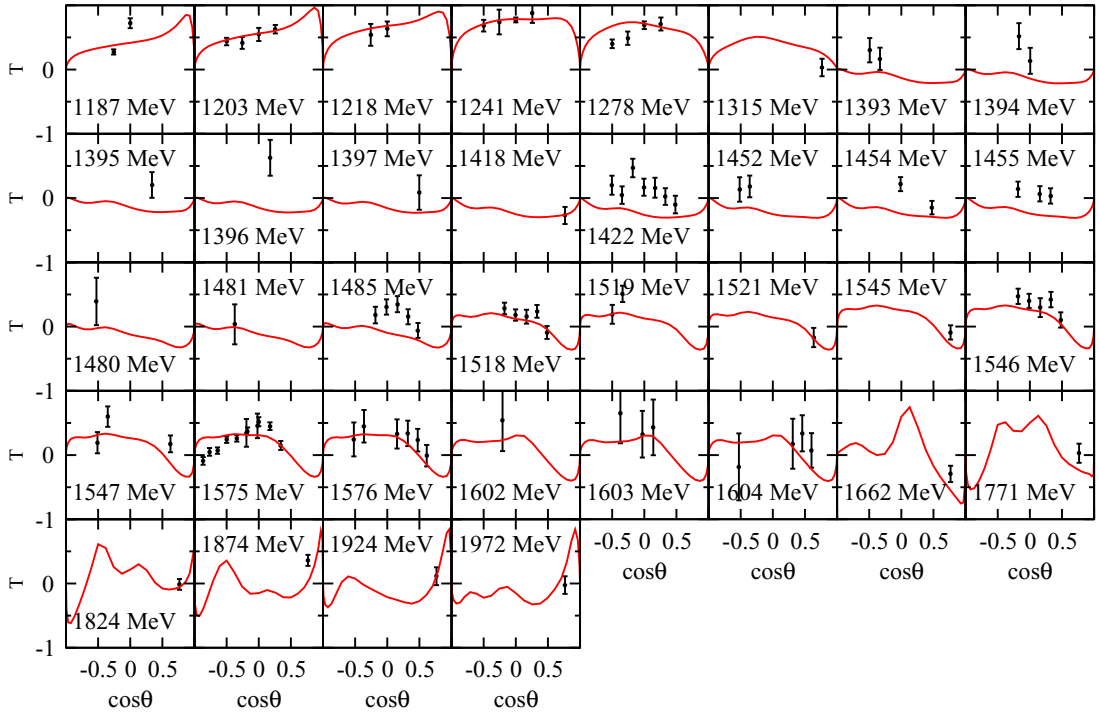

FIG. 5. Result of fit for T of $\gamma\,'n' \to \pi^- p$.

$$A_{1/2} = N R_{\pi N \gamma N(1/2)}, \tag{18}$$

$$N = a\sqrt{\frac{k_{\pi N}^{\rm on}}{K}\frac{2\pi(2J^R+1)M_R}{m_N R_{\pi N,\pi N}}}, \tag{19}$$

with $a = \sqrt{2/3}$ for $I = \frac{3}{2}$ N^* and $a = -\sqrt{3}$ for $I = \frac{1}{2}$ N^*; the phase is fixed so that $-\pi/2 \leqslant \arg(N/a) \leqslant \pi/2$.

III. COMBINED ANALYSIS OF MESON PRODUCTIONS OFF PROTON AND NEUTRON TARGETS

In this work, we do combined fits to the data for both the proton- and neutron-target reactions. The same database as used in our previous work [5] is employed for the proton-target reactions, $\pi p \to MB$ and $\gamma p \to MB$ with $MB = \pi N$, ηN, $K\Lambda$, $K\Sigma$, while for the neutron-target reactions we include ~3200 data points of $\gamma\,'n' \to \pi N$ as summarized in Table I (where 'n' represents the neutron bound in the deuteron).

The fitting procedures are the same as explained in Ref. [5] and will not be repeated here. The results of our fits to the data for the neutron-target reactions are presented in Sec. III A. As for the fits to the much more extensive data for the proton-target reactions, however, we only present a small sample of the selected results in Sec. III B to indicate the differences with our fits presented in Ref. [5]. The values of determined model parameters are given in the Supplemental Material [28].

A. Fits to data for neutron-target reactions

The results of our fits to the $\gamma\,'n' \to \pi^- p$ data are presented in Figs. 2 and 3 for the differential cross section $d\sigma/d\Omega$, Fig. 4 for the photon asymmetry Σ, Fig. 5 for the target polarization T, and Fig. 6 for the recoil polarization P. Clearly, the results are reasonably good in the energy region considered up to $W = 2$ GeV. However, it should be noted that more data for polarization observables would be highly desirable to determine $\gamma n \to N^*$ transition amplitudes. In this regard, a number of new data for meson photoproductions using the polarized photon beam and/or the polarized deuteron target will be available soon from the electron- and photon-beam facilities such as the Thomas Jefferson National Accelerator Facility, the Electron Stretcher Accelerator at Bonn, and the Mainz Microtron. The main purpose of these experimental efforts is to obtain precise data for the "(over-)complete" set of observables for the $\gamma\,'n' \to MB$ reactions with $MB = \pi N$, ηN, $K\Lambda$, $K\Sigma, \ldots$, which, together with the data of the reactions on the proton target, are crucial for obtaining definitive information for the isospin structure of photoexcitation amplitudes of the nucleon. For reference, in Fig. 7 we present the results of all 16 observables for the $\gamma\,'n' \to \pi^- p$ reaction at $W = 1662$ MeV and $W = 1924$ MeV, which respectively correspond to $E_\gamma = 1$ GeV and $E_\gamma = 1.5$ GeV with E_γ being the incoming photon energy in the laboratory frame. The calculated results of all observables for $\gamma n \to \pi^- p$ as well as $\gamma n \to \pi^0 n$ for $W \leqslant 2$ GeV are available upon request.

While the results of our fits to the $\gamma\,'n' \to \pi^- p$ data are reasonably good, we also see some deviations of our curves from the data points at several energies. One reason for this would be due to an inconsistency between different data sets. For example, there are significant differences between the $d\sigma/d\Omega$ data at $W = 1240$ and 1241 MeV in magnitude for $\cos\theta > 0$, even though they have just 1 MeV difference in W. These two data sets were extracted from the $\gamma d \to \pi^- pp$

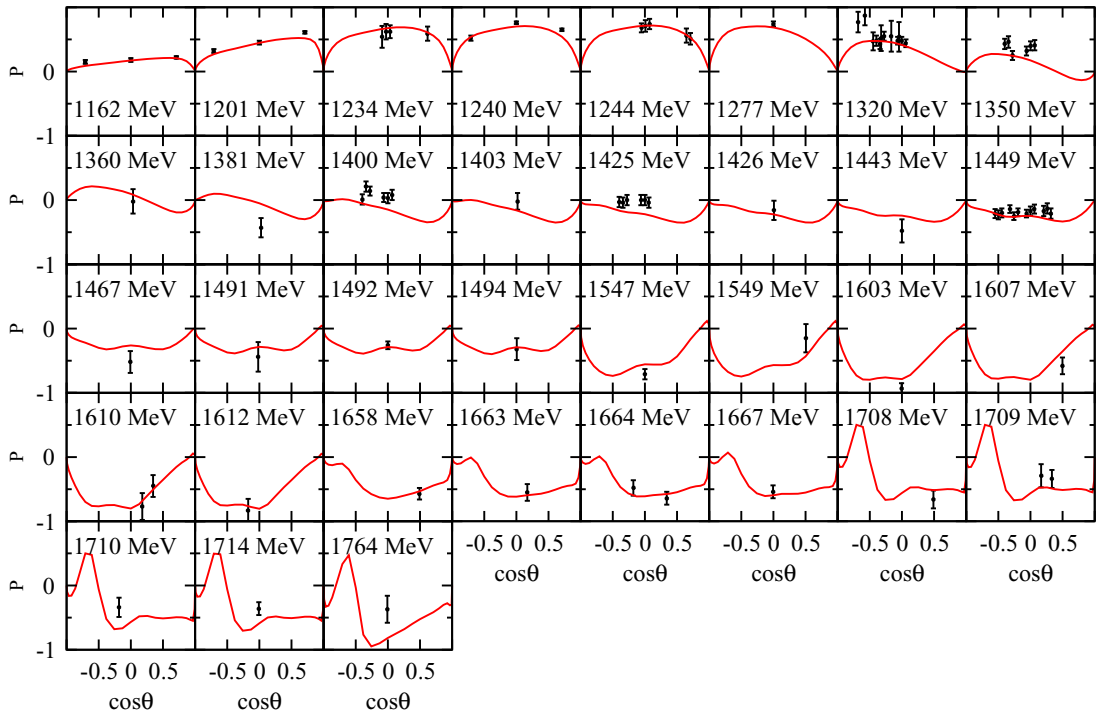

FIG. 6. Result of fit for P of $\gamma\,'n' \to \pi^- p$.

reaction by different experiments and analysis groups in Ref. [29] and in Refs. [30–32], respectively. This kind of inconsistency could arise from the differences in the methods employed for extracting the information on the $\gamma\,'n'$ reactions from the γd reactions, e.g., the momentum cuts taken for the data selection and/or the initial- and final-state interactions taken into account, etc. The $\gamma\,'n' \to \pi N$ data are thus "biased" by the analysis methods employed. To avoid such inconsistency, ideally one should directly analyze the original γd reaction data. Nevertheless, as a first step toward a reliable extraction of the $\gamma n \to N^*$ amplitudes, we follow the previous analyses by using the available $\gamma\,'n' \to \pi N$ data in this work. The model parameters obtained in this work are then used as starting values for the γd analysis that will be presented elsewhere.

Our fits to the $\gamma\,'n' \to \pi^0 n$ data are shown in Fig. 8 for $d\sigma/d\Omega$ and in Fig. 9 for Σ. Here we see that the data for $d\sigma/d\Omega$ are very limited, while reasonably good fits to the Σ data are achieved. The $\gamma\,'n' \to \pi^0 n$ data are usually extracted from the $\gamma d \to \pi^0 pn$ reaction. However, the $\gamma d \to \pi^0 pn$ process

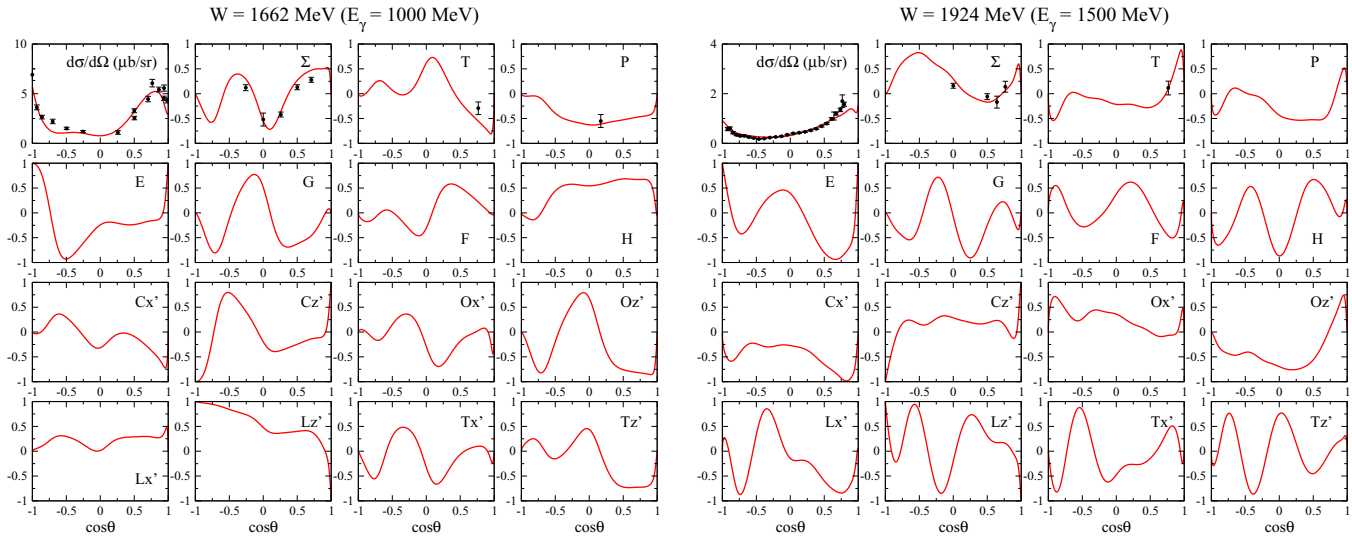

FIG. 7. Differential cross section and all polarization observables for $\gamma\,'n' \to \pi^- p$. The left panels [right panels] are the results at $W = 1662$ MeV($E_\gamma = 1000$ MeV)[$W = 1924$ MeV($E_\gamma = 1500$ MeV)]. The results for the observables for which no data are presented are predictions from our current DCC model.

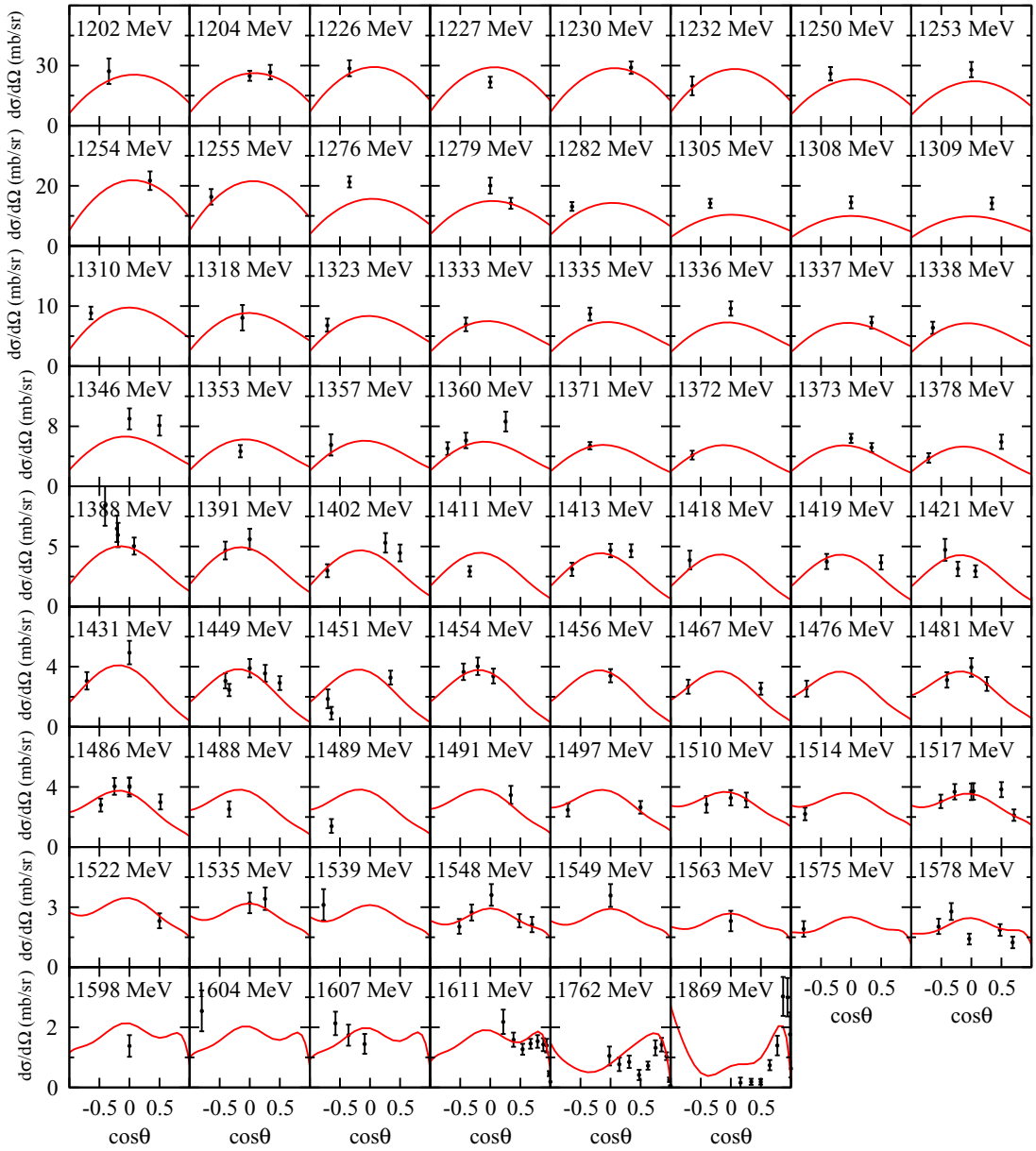

FIG. 8. Result of fit for $d\sigma/d\Omega$ of $\gamma\,'n' \to \pi^0 n$.

is more complicated than $\gamma d \to \pi^- pp$ because the final-state interactions between the outgoing pn pair are expected to be more sizable, as demonstrated, e.g., in the study [33] of the $\gamma d \to \pi NN$ and $\nu d \to l\pi NN$ reactions in the $\Delta(1232)$ resonance region. To improve the fits to the data with $\pi^0 n$ final state, it would be more essential to directly analyze the γd reactions within our DCC approach in a fully consistent way, rather than using the $\gamma\,'n' \to \pi N$ data extracted by other experiments or analysis groups.

B. Fits to data for proton-target reactions

Since the amount of data for the proton-target reactions is much greater than for the neutron-target reactions, our model parameters determined in this work are still mainly constrained by the proton-target reactions, except for those associated with the $\gamma n \to N^*$ transitions. Accordingly, the quality of the fits to the data for the proton-target reactions is similar to the results we presented in Ref. [5] (hereafter we refer to the model of Ref. [5] as "the 2013 model"). Nevertheless, there are some differences that are worth mentioning:

(1) Figure 10 shows the total cross sections for the $\gamma p \to \pi N$ and inclusive $\gamma p \to X$ reactions, where the solid and dashed curves are given by the DCC model of this work and the 2013 model [5], respectively. We see that both models give almost the same cross sections for $\gamma p \to \pi N$. However, it turns out that the $\gamma p \to X$ total cross section predicted with the 2013 model [5] visibly overestimates (underestimates) the data at $1.55 \lesssim W \lesssim 1.8$ GeV ($1.4 \lesssim W \lesssim 1.5$ GeV). This deviation from the data is mostly due to the

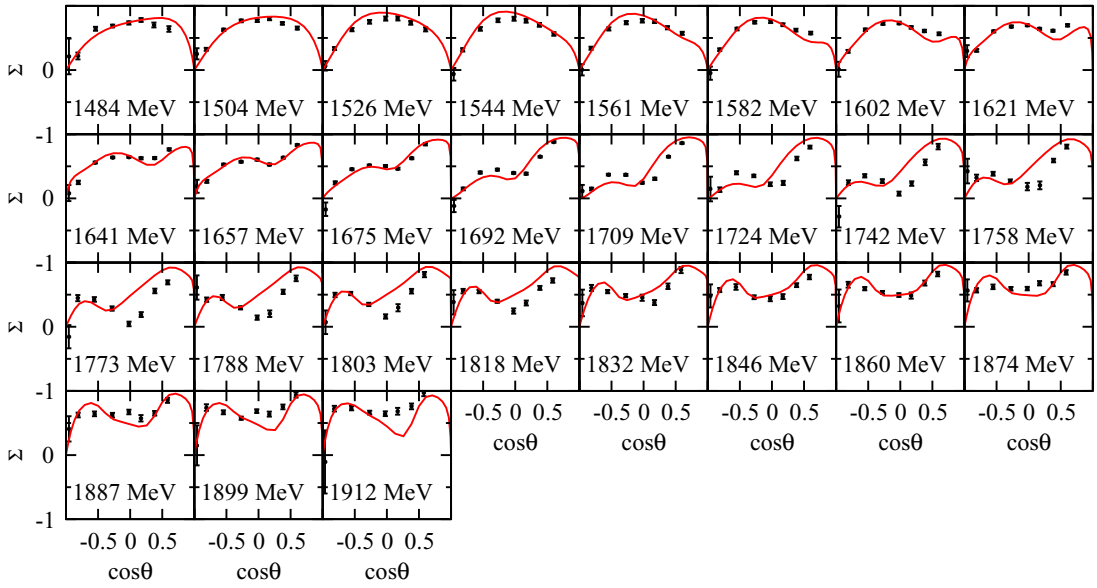

FIG. 9. Result of fit for Σ of γ'n' $\to \pi^0 n$.

uncertainty of the $\gamma N \to \pi\Delta$, σN, $\rho N \to \pi\pi N$ processes because at present we have included only the $\gamma p \to \pi N, \eta N, K\Lambda, K\Sigma$ data in our analysis and the $\pi\pi N$ production processes are indirectly constrained through the coupled-channels effect. To eliminate the deviation from the data mentioned above, in this work we included the data for $\gamma p \to X$ total cross section at $W \lesssim 1.75$ GeV into our analysis. As a result, the overestimation of the $\gamma p \to X$ total cross section at $1.55 \lesssim W \lesssim 1.8$ GeV has been improved significantly in our current model. However, the underestimation at $1.4 \lesssim W \lesssim 1.5$ GeV still remains although some improvements are observed. To resolve this underestimation, we would need to extend our analysis by including the $\gamma N \to \pi\pi N$ data and by adding some new nonresonant mechanisms for $\gamma N \to \pi\pi N$. This requires tremendous efforts and time-consuming numerical tasks, so we leave it for our future work.

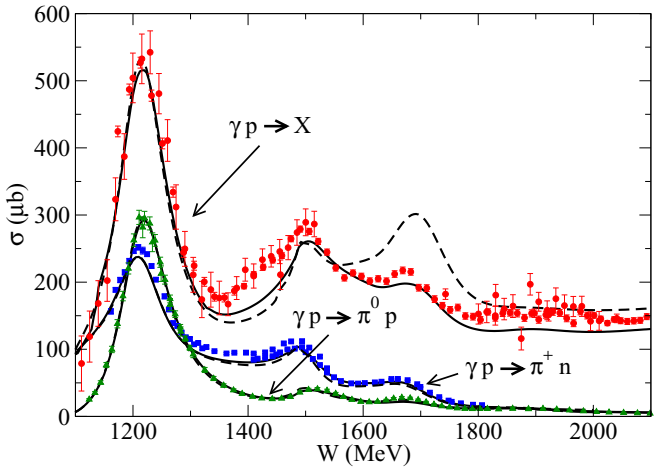

FIG. 10. Total cross sections for the inclusive $\gamma p \to X$ and $\gamma p \to \pi N$ reactions. Solid curves are the results from the current analysis, while the dashed curves are the ones obtained from the 2013 model [5].

(2) In Fig. 11, the results of the fits from this work and the 2013 model [5] are presented for $d\sigma/d\Omega$ and Σ of $\gamma p \to \pi^0 p$. Overall, a significant improvement has been achieved for these observables in the high-W region with $W \gtrsim 1.87$ GeV. We further find that the improvements for $d\sigma/d\Omega$ are made mostly in the forward-angle region, in which the t-channel vector-meson exchange processes dominate the cross sections and thus mainly contribute to the improvement. On the other hand, the results of fits for Σ are improved over almost the entire range of $\cos\theta$, which means that model parameters associated with bare N^* states are also modified significantly. As a result, values of the $\gamma p \to N^*$ transition amplitudes for high-mass N^* resonances are significantly modified as well, as discussed in Sec. IV.

(3) In Fig. 12, the results of the fits from this work and the 2013 model [5] are presented for $d\sigma/d\Omega$ ($1.4 \lesssim W \lesssim 1.5$ GeV) and Σ ($1.77 \lesssim W \lesssim 2.1$ GeV) of $\gamma p \to \pi^+ n$. Similarly to the $\gamma p \to \pi^0 p$ case, the results for $d\sigma/d\Omega$ are improved particularly in the forward region, while the improvement for Σ extends over the entire $\cos\theta$ region.

The fits to the data of the production of $K\Lambda$ and $K\Sigma$ off the proton target have also been improved significantly both for photon- and pion-induced reactions. This is, however, not very relevant to the purpose of this paper and will not be presented here.

IV. EXTRACTED RESONANCE PARAMETERS

We now turn to discuss the extracted N^* resonance parameters, which are defined at the poles of the scattering

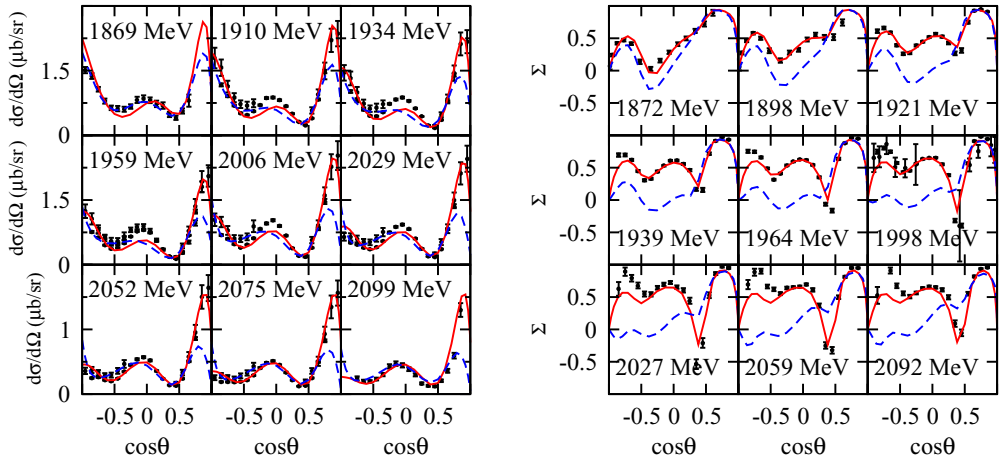

FIG. 11. $d\sigma/d\Omega$ (left panels) and Σ (right panels) of $\gamma p \to \pi^0 p$. Red solid curves (blue dashed curves) are the result from the current analysis (the 2013 model [5]).

amplitudes in the complex W plane. In Table II, we list the pole mass M_R and πN elastic residue $R_{\pi N,\pi N}$ for each extracted N^* resonance. Here the corresponding results of the 2013 model [5] are also presented for a comparison. Overall, no significant difference is found in the results between the two models, implying that pole positions and coupling strengths to the πN channel are more or less well determined for N^* resonances below $W = 2$ GeV. However, some difference can also be seen for the N^* resonances with large imaginary parts for M_R, such as the P_{31} and D_{35} resonances and the second P_{11}, P_{33}, D_{33} resonances. This would reflect the fact that analysis dependence comes more into N^* resonances located far from the physical real energy axis and their parameters are in practice less well determined, although in principle the pole parameters should be unique. In particular, we do not find the second D_{33} resonance in the current work, suggesting that the pole of this resonance has disappeared or moved far away from the complex-W region close to the physical real energy axis. One can see qualitatively that there are some correlations in the change of values between $\mathrm{Im}(M_R)$ and $R_{\pi N,\pi N}$, i.e., a larger change in $\mathrm{Im}(M_R)$ leads to a larger change in $R_{\pi N,\pi N}$. This is perhaps related to the fact that the contribution of a resonance to the πN partial-wave amplitude is roughly determined by the ratio $-iR_{\pi N,\pi N}/\mathrm{Im}(M_R)$ at $W \sim \mathrm{Re}(M_R)$. Since the πN partial-wave amplitudes are well determined and exhibit almost no difference between the current and 2013 models, the values of the $R_{\pi N,\pi N}$ residues tend to vary to "compensate" the change in the extracted values of $\mathrm{Im}(M_R)$ such that the total πN partial-wave amplitudes remain the same.

In Table III, we compare the helicity amplitudes for the $\gamma p \to N^*$ transition evaluated at the resonance pole positions. The notation of the presented values follows that used in Ref. [16]. In contrast to the πN elastic residue $R_{\pi N,\pi N}$, visible differences from the 2013 model are observed for most of the helicity amplitudes, except for the very-well-established resonances, such as the first P_{33} and S_{11} resonances. This is due to the significant improvement in the fits to the γp reaction data in this work, as seen in Figs. 10–12. In particular, it is found that the change in the helicity amplitudes for N^* resonances

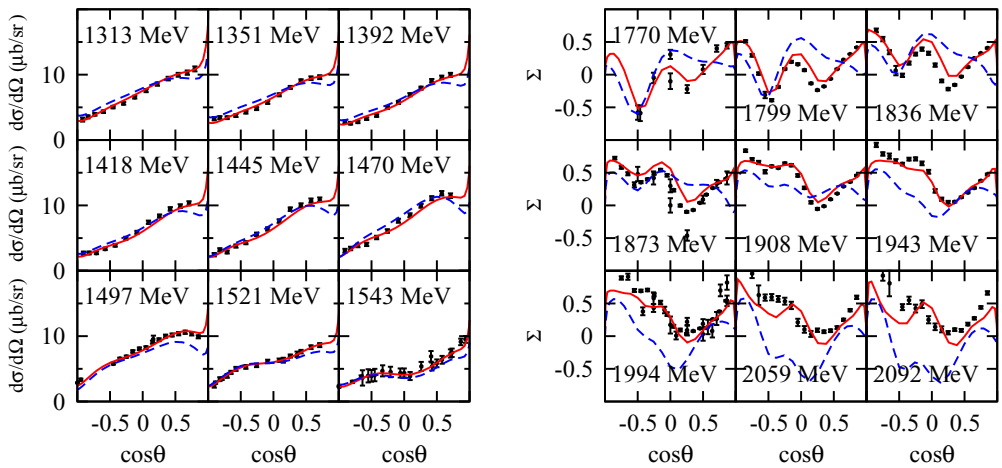

FIG. 12. $d\sigma/d\Omega$ (left panels) and Σ (right panels) of $\gamma p \to \pi^+ n$. Red solid curves (blue dashed curves) are the result from the current analysis (our previous model [5]).

TABLE II. Comparison of N^* pole mass M_R and πN elastic residue $R_{\pi N,\pi N}$ between this work and the 2013 model [5]. M_R is listed as $(\mathrm{Re}(M_R), -\mathrm{Im}(M_R))$ in units of MeV, while $R_{\pi N,\pi N} = |R_{\pi N,\pi N}|e^{i\phi}$ is listed as $(|R_{\pi N,\pi N}|, \phi)$ in units of MeV for $|R_{\pi N,\pi N}|$ and degree for ϕ. The range of ϕ is taken to be $-180^\circ \leqslant \phi < 180^\circ$. The N^* resonances for which the asterisk (*) is marked locate in the complex energy plane slightly off the sheet closest to the physical real energy axis, yet are still expected to visibly affect the physical observables.

		M_R		$R_{\pi N,\pi N}$	
	$J^P(L_{2I2J})$	This work	2013 model	This work	2013 model
N baryons	$1/2^-(S_{11})$	(1490,102)	(1482,98)*	(70,−42)	(63,−44)
		(1652,71)	(1656,85)	(45,−74)	(53,−70)
	$1/2^+(P_{11})$	(1376,75)	(1374,76)	(38,−70)	(37,−69)
		(1741,139)	(1746,177)	(15,80)	(20,3)
	$3/2^+(P_{13})$	(1708,65)	(1703,70)	(9,−4)	(8,−3)
		(1765,160)	(1763,159)	(30,−105)	(29,−106)
	$3/2^-(D_{13})$	(1509,48)	(1501,39)	(31,−10)	(26,−11)
		(1702,148)*	(1702,141)*	(<1,161)	(2,104)
	$5/2^-(D_{15})$	(1651,68)	(1650,75)	(26,−27)	(28,−31)
	$5/2^+(F_{15})$	(1665,52)	(1665,49)	(36,−22)	(34,−20)
Δ baryons	$1/2^-(S_{31})$	(1597,69)	(1592,68)	(21,−111)	(20,−111)
		(1713,187)	(1702,193)	(20,73)	(19,65)
	$1/2^+(P_{31})$	(1857,145)	(1854,184)	(11,−118)	(23,−123)
	$3/2^+(P_{33})$	(1212,52)	(1211,51)	(55,−47)	(53,−47)
		(1733,162)	(1734,176)	(16,−108)	(8,−118)
	$3/2^-(D_{33})$	(1577,113)	(1592,122)	(13,−67)	(18,−62)
			(1707,170)*		(11,49)
	$5/2^-(D_{35})$	(1911,130)	(1936,105)	(4,−30)	(2,−32)
	$5/2^+(F_{35})$	(1767,88)	(1765,94)	(11,−61)	(11,−62)
	$7/2^+(F_{37})$	(1885,102)	(1872,103)	(49,−30)	(46,−35)

TABLE III. Comparison of helicity amplitudes for the $\gamma p \to N^*$ transition obtained from this work and from the 2013 model [5]. The values presented follow the notation in Ref. [16], i.e., $A_{1/2,3/2} = \bar{A}_{1/2,3/2} \times e^{i\phi}$ with ϕ taken to be in the range $-90^\circ \leqslant \phi < 90^\circ$. The units of $\bar{A}_{1/2,3/2}$ and ϕ are 10^{-3} GeV$^{-1/2}$ and degrees, respectively. Each resonance is specified by the isospin and spin-parity quantum numbers as well as the real part of the resonance pole mass.

	$A_{1/2}$				$A_{3/2}$			
	This work		2013 model		This work		2013 model	
Particle $J^P(L_{2I2J})$	$\bar{A}_{1/2}$	ϕ	$\bar{A}_{1/2}$	ϕ	$\bar{A}_{3/2}$	ϕ	$\bar{A}_{3/2}$	ϕ
$N(1490)1/2^-(S_{11})$	160	8	161	9				
$N(1652)1/2^-(S_{11})$	36	−28	40	−44				
$N(1376)1/2^+(P_{11})$	−40	−8	−50	−12				
$N(1741)1/2^+(P_{11})$	−47	−24	86	−74				
$N(1708)3/2^+(P_{13})$	131	7	234	2	−33	12	−70	−7
$N(1765)3/2^+(P_{13})$	123	−11	145	−30	−71	3	−44	−1
$N(1509)3/2^-(D_{13})$	−28	<1	−38	3	101	4	94	7
$N(1703)3/2^-(D_{13})$	13	50	26	64	31	−71	54	−42
$N(1651)5/2^-(D_{15})$	8	19	5	−22	49	−12	33	−23
$N(1665)5/2^+(F_{15})$	−44	−11	−53	−5	60	−2	38	3
$\Delta(1597)1/2^-(S_{31})$	105	1	113	−1				
$\Delta(1713)1/2^-(S_{31})$	40	13	35	5				
$\Delta(1857)1/2^+(P_{31})$	−1	−78	52	−10				
$\Delta(1212)3/2^+(P_{33})$	−134	−16	−133	−15	−257	−3	−257	−3
$\Delta(1733)3/2^+(P_{33})$	−48	63	−72	71	−94	74	−136	82
$\Delta(1577)3/2^-(D_{33})$	128	19	129	17	119	46	117	41
$\Delta(1911)5/2^-(D_{35})$	48	−22	53	−21	11	−36	35	−15
$\Delta(1767)5/2^+(F_{35})$	38	−7	8	83	−24	−80	−18	−90
$\Delta(1885)7/2^+(F_{37})$	−69	−14	−62	−9	−83	2	−76	2

TABLE IV. Comparison of our helicity amplitudes for the $\gamma n \to N^*$ transition with those extracted by Bonn–Gatchina (BoGa) analysis [16]. See the caption of Table III for the notation of the table. No resonances corresponding to $N(1765)3/2^+$ and $N(1703)3/2^-$ are found in BoGa.

	$A_{1/2}$				$A_{3/2}$			
	This work		BoGa		This work		BoGa	
Particle $J^P(L_{2I2J})$	$\bar{A}_{1/2}$	ϕ	$\bar{A}_{1/2}$	ϕ	$\bar{A}_{3/2}$	ϕ	$\bar{A}_{3/2}$	ϕ
$N(1490)1/2^-(S_{11})$	-112	16	-103 ± 11	8 ± 5				
$N(1652)1/2^-(S_{11})$	-1	-47	25 ± 20	0 ± 15				
$N(1376)1/2^+(P_{11})$	95	-15	35 ± 12	25 ± 25				
$N(1741)1/2^+(P_{11})$	195	-8	-40 ± 20	-30 ± 25				
$N(1708)3/2^+(P_{13})$	-59	6	-80 ± 50	-20 ± 30	-28	-19	-140 ± 65	5 ± 30
$N(1765)3/2^+(P_{13})$	-34	-5			40	6		
$N(1509)3/2^-(D_{13})$	-43	-1	-49 ± 8	-3 ± 8	-110	5	-114 ± 12	1 ± 3
$N(1703)3/2^-(D_{13})$	-40	-46			-77	-57		
$N(1651)5/2^-(D_{15})$	-76	3	-61 ± 7	-10 ± 5	-38	-4	-89 ± 10	-17 ± 7
$N(1665)5/2^+(F_{15})$	34	-12	33 ± 6	-12 ± 9	-56	-4	-44 ± 9	8 ± 10

with the mass $M_R \sim 1.7$ GeV, in particular for $N(1708)3/2^+$, originates mostly from reducing the overestimation of the $\gamma p \to X$ total cross sections in our previous 2013 model (Fig. 10). We also observe that the improvement in fitting the polarization observables for $\gamma p \to \pi N$, ηN, $K\Lambda$, $K\Sigma$ reactions at $W \gtrsim 1.8$ GeV (the right panels of Figs. 11 and 12 for the case of Σ for $\gamma p \to \pi N$) is related to the changes in the helicity amplitudes of the higher N^* resonances. It is worth mentioning that the $N(1651)5/2^-$ resonance has small $\bar{A}_{1/2}$, while the value of $\bar{A}_{3/2}$ is rather large. In a constituent quark model, this N^* state is assigned as a member of the $[\mathbf{70},^4 8]$ representation of SU(6)×O(3), and thus the $\gamma p \to N^*$ transition amplitudes are exactly zero [34]. However, we find that, within the current DCC model, the large nonzero value of $A_{3/2}$ for the $N(1651)5/2^-$ resonance mostly comes from the bare N^* contribution. This seems to be in contradiction with the above argument based on the naive quark-model and a discussion made in Ref. [35].

One can see from Table III that the $\gamma p \to N^*$ transition amplitudes defined by poles are essentially complex. Thus they differ from the helicity amplitudes listed by Particle Data Group (PDG) [36], which are from fits using the Breit–Wigner parametrization and the resulting values are real by definition. According to a resonance theory based on the Gamow vectors (see, e.g., Ref. [37]), the transition amplitudes defined with the residues at poles of the scattering amplitudes are transition-matrix elements associated with the exact complex-energy eigenstates of the full Hamiltonian of the considered system obtained under the purely outgoing boundary condition. Thus the transition amplitudes defined by poles have a clear connection to the underlying theory (i.e., QCD), while the phenomenological Breit–Wigner parameters do not. If the phase ϕ of the transition amplitudes is small, the Breit–Wigner amplitudes can be a good approximation of the pole amplitudes. In fact, our DCC model gives $\bar{A}_{1/2} = -0.133$ GeV$^{-1/2}$ and $\bar{A}_{3/2} = -0.257$ GeV$^{-1/2}$ for the first P_{33} resonance, while the (real) Breit–Wigner amplitudes are $A_{1/2} = -0.135 \pm 0.006$ GeV$^{-1/2}$ and $A_{1/2} = -0.255 \pm 0.005$ GeV$^{-1/2}$ [36]. However, if ϕ is large, there exists no clear relation between them. This argument is of course applicable also to the $\gamma n \to N^*$ transition amplitudes.

The extracted $\gamma n \to N^*$ transition amplitudes are listed in Table IV. Here only the results for the isospin $I = 1/2$ nucleon resonances are presented because $\gamma p \to \Delta^*$ and $\gamma n \to \Delta^*$ give the same value. In the same table, we also present the results obtained by the Bonn–Gatchina (BoGa) analysis [16] for a comparison. The results from ours and BoGa show a reasonable agreement for the transition amplitudes, for which the BoGa analysis assigns relatively small uncertainties for the extracted amplitudes. In particular, our results for the first S_{11}, D_{13}, and F_{15} resonances, which correspond respectively to $N(1535)1/2^-$, $N(1520)3/2^-$, and $N(1680)5/2^+$ in the PDG notation, are in good agreement with the BoGa results. However, some disagreement is also seen for several N^* resonances. The BoGa analysis gives positive $\bar{A}_{1/2}$ for the second S_{11} resonance, while in our analysis $\bar{A}_{1/2}$ is negative and very small. To obtain a more conclusive result for this transition amplitude, however, we would also need to take into account ηn photoproduction data, as discussed in Ref. [16]. We hope to make this extended analysis by directly analyzing $\gamma d \to \eta p n$ reactions, rather than analyzing the γ'n' $\to \eta n$ data provided by other experiment or analysis groups, and this will be presented elsewhere. The origin of a significant disagreement in the transition amplitudes for the P_{11} resonances would also come from a couple of reasons: (a) The pole mass of the second P_{11} resonance from two analyses is different; i.e., $M_R = 1741 - i139$ MeV from our analysis and $M_R = 1687 - i100$ MeV from BoGa. Since the value of the residue has a strong correlation with the pole mass and is more sensitive to the analysis model used in each analysis, one should first well determine the pole mass to accomplish a precise determination of the residues. (b) The P_{11} resonances are found to give a small contribution to the $\gamma n \to \pi N$ reactions within our DCC model, and thus the $\gamma n \to N^*$ transition amplitudes are not well constrained by the $\gamma n \to \pi N$ data. Therefore, to get more convergent results, we would need to further include the data associated with the other meson photoproductions off the neutron, such as $\pi\pi$,

TABLE V. The isovector and isoscalar helicity amplitudes for $\gamma N \to N^*$, as defined by Eqs. (20) and (21). See the caption of Table III for the notation used in the table.

	$A^{T=1}_{1/2}$		$A^{T=0}_{1/2}$		$A^{T=1}_{3/2}$		$A^{T=0}_{3/2}$	
Particle $J^P(L_{2I2J})$	$\bar{A}^{T=1}_{1/2}$	ϕ	$\bar{A}^{T=0}_{1/2}$	ϕ	$\bar{A}^{T=1}_{3/2}$	ϕ	$\bar{A}^{T=0}_{3/2}$	ϕ
$N(1490)1/2^-(S_{11})$	136	11	26	−10				
$N(1652)1/2^-(S_{11})$	19	−29	18	−28				
$N(1376)1/2^+(P_{11})$	−68	−13	28	−21				
$N(1741)1/2^+(P_{11})$	−120	−11	75	−3				
$N(1708)3/2^+(P_{13})$	95	7	36	8	−9	68	−29	−2
$N(1765)3/2^+(P_{13})$	78	−10	45	−14	−55	4	−16	−2
$N(1509)3/2^-(D_{13})$	7	−2	−35	−1	106	4	−5	8
$N(1703)3/2^-(D_{13})$	20	−28	−22	−63	54	−61	−24	−48
$N(1651)5/2^-(D_{15})$	42	4	−34	1	44	−8	6	−37
$N(1665)5/2^+(F_{15})$	−39	−11	−5	−8	58	−3	2	18

η, and K productions, into our fits to get convergent results. However, as already mentioned, this is beyond the scope of the current work and will be performed elsewhere.

Combining the $\gamma n \to N^*$ and $\gamma p \to N^*$ transition amplitudes listed in Tables III and IV, we can obtain the isovector ($T = 1$) and isoscalar ($T = 0$) parts of the $\gamma N \to N^*$ amplitude for $I = 1/2 N^*$ by using the following well-known relations:

$$A^{T=1}_{\lambda} = \left(A^{1/2p}_{\lambda} - A^{1/2n}_{\lambda}\right)/2, \tag{20}$$

$$A^{T=0}_{\lambda} = \left(A^{1/2p}_{\lambda} + A^{1/2n}_{\lambda}\right)/2, \tag{21}$$

where $A^{1/2p}_{\lambda}$ and $A^{1/2n}_{\lambda}$ are helicity amplitudes for $\gamma p \to N^*$ and $\gamma n \to N^*$ transitions, respectively. The resulting values of the isospin-decomposed transition amplitudes within our current DCC analysis are presented in Table V as a reference.

V. SUMMARY AND DISCUSSIONS

In this work, we have extended our DCC analysis [5] of the $\pi p, \gamma p \to \pi N$, ηN, $K\Lambda$, $K\Sigma$ reactions by further including the data for pion photoproductions off the neutron target, $\gamma n \to \pi N$, in the fits. The helicity amplitudes for the $\gamma n \to N^*$ transition, defined by the residues of the poles of the scattering amplitudes, have then been extracted. Through this combined analysis of both the proton- and neutron-target reactions, the resonance pole masses and the $\gamma p \to N^*$ transition amplitudes extracted from our previous analysis [5] have also been revised accordingly. Our results allow an isospin decomposition of the $\gamma N \to N^*$ transitions, which is needed for testing the hadron structure calculations and investigating the neutrino-induced reactions [14]. The extracted $\gamma n \to N^*$ transition amplitudes are compared with the results of the BoGa analysis. It is found that two results are consistent with each other overall. However, some significant disagreements also exist for several N^* resonances, implying that further extensions of both analyses to analyze more complete data on the neutron target will be needed to make progress.

As mentioned throughout this paper, in our current analysis we have used the γ'n' $\to \pi N$ data extracted from the $\gamma d \to \pi NN$ data by other experiments and analysis groups. In most experimental analyses, the $\gamma n \to \pi N$ cross sections and polarization observables are extracted by simply applying momentum cuts to the deuteron data and choosing the kinematics where the quasifree mechanisms are assumed to dominate the reaction processes. Effects of the nucleon Fermi motion inside the deuteron have also been included in some analyses, but final πNN interactions are usually neglected. On the other hand, several theoretical investigations [33,38–41] have shown that the πNN final-state interaction has very large effects on the $\gamma d \to \pi^0 pn$ reaction. Similar large effects are expected also for the other neutral-meson productions such as $\gamma d \to M^0 pn$ with $M^0 = \eta, \eta', \omega, \phi, \ldots$. To make further progress in the study of the N^* spectroscopy, an approach for investigating these meson production reactions off the deuteron must be developed. Since the accuracy of the extracted $\gamma n \to \pi N$ data depends on the way of unfolding the many-body effects from the raw data, it is highly desirable to analyze directly the data of $\gamma d \to \pi NN$ reactions based on a well-developed reaction model. The DCC model employed in our analysis is particularly useful for the analysis of γ-d and also γ-nuclei reactions since the necessary off-shell amplitudes are readily available. To complete such a analysis, a method to describe the πNN dynamics in the Δ and higher N^* resonance region has to be explored. These necessary tasks towards determining electromagnetic interactions associated with the N^* resonances will be taken step by step and presented elsewhere.

ACKNOWLEDGMENTS

This work was supported by the Japan Society for the Promotion of Science (JSPS) KAKENHI Grants No. 25800149 (H.K.) and No. 16K05354 (T.S.), the MEXT KAKENHI Grant No. 25105010 (T.S.), and by the US Department of Energy, Office of Nuclear Physics Division, under Contract No. DE-AC02-06CH11357. This research used resources of the National Energy Research Scientific Computing Center, which is supported by the Office of Science of the US Department of Energy under Contract No. DE-AC02-05CH11231, and resources provided on Blues and/or Fusion, high-performance computing cluster operated by the Laboratory Computing Resource Center at Argonne National Laboratory.

[1] R. L. Workman, M. W. Paris, W. J. Briscoe, and I. I. Strakovsky, Phys. Rev. C **86**, 015202 (2012); R. L. Workman, R. A. Arndt, W. J. Briscoe, M. W. Paris, and I. I. Strakovsky, *ibid.* **86**, 035202 (2012).

[2] A. V. Anisovich, R. Beck, E. Klempt, V. A. Nikonov, A. V. Sarantsev, and U. Thoma, Eur. Phys. J. A **48**, 15 (2012).

[3] V. Shklyar, H. Lenske, U. Mosel, and G. Penner, Phys. Rev. C **71**, 055206 (2005).

[4] T. P. Vrana, S. A. Dytman, and T.-S. H. Lee, Phys. Rep. **328**, 181 (2000).

[5] H. Kamano, S. X. Nakamura, T.-S. H. Lee, and T. Sato, Phys. Rev. C **88**, 035209 (2013).

[6] D. Rönchen, M. Döring, H. Haberzettl, J. Haidenbauer, U.-G. Meißner, and K. Nakayama, Eur. Phys. J. A **51**, 70 (2015); D. Rönchen, M. Döring, F. Huang, H. Haberzettl, J. Haidenbauer, C. Hanhart, S. Krewald, U.-G. Meißner, and K. Nakayama, *ibid.* **50**, 101 (2014); **49**, 44 (2013).

[7] L. Tiator, S. S. Kamalov, S. Ceci, G. Y. Chen, D. Drechsel, A. Svarc, and S. N. Yang, Phys. Rev. C **82**, 055203 (2010); G. Y. Chen, S. S. Kamalov, S. N. Yang, D. Drechsel, and L. Tiator, *ibid.* **76**, 035206 (2007).

[8] V. D. Burkert and T. S. H. Lee, Int. J. Mod. Phys. E **13**, 1035 (2004).

[9] B. Juliá-Díaz, T.-S. H. Lee, T. Sato, and L. C. Smith, Phys. Rev. C **75**, 015205 (2007).

[10] B. Juliá-Díaz, T.-S. H. Lee, A. Matsuyama, T. Sato, and L. C. Smith, Phys. Rev. C **77**, 045205 (2008).

[11] B. Juliá-Díaz, H. Kamano, T.-S. H. Lee, A. Matsuyama, T. Sato, and N. Suzuki, Phys. Rev. C **80**, 025207 (2009).

[12] N. Suzuki, T. Sato, and T.-S. H. Lee, Phys. Rev. C **82**, 045206 (2010).

[13] R. Gothe *et al.*, Nucleon Resonance Studies with CLAS12 (JLab E12-09-003), https://www.jlab.org/exp_prog/proposals/09/PR12-09-003.pdf; D. S. Carman *et al.*, Exclusive $N^* \to KY$ Studies with CLAS12 (JLab E12-06-108A), https://www.jlab.org/exp_prog/proposals/14/E12-06-108A.pdf.

[14] S. X. Nakamura, H. Kamano, and T. Sato, Phys. Rev. D **92**, 074024 (2015).

[15] F. Huang, M. Döring, H. Haberzettl, J. Haidenbauer, C. Hanhart, S. Krewald, U. G. Meißner, and K. Nakayama, Phys. Rev. C **85**, 054003 (2012).

[16] A. V. Anisovich, V. Burkert, E. Klempt, V. A. Nikonov, A. V. Sarantsev, and U. Thoma, Eur. Phys. J. A **49**, 67 (2013).

[17] A. Matsuyama, T. Sato, and T.-S. H. Lee, Phys. Rep. **439**, 193 (2007).

[18] M. Kobayashi, T. Sato, and H. Ohtsubo, Prog. Theor. Phys. **98**, 927 (1997).

[19] T. Sato and T.-S. H. Lee, J. Phys. G **36**, 073001 (2009).

[20] H. Feshbach, *Theoretical Nuclear Physics, Nuclear Reactions* (Wiley, New York, 1992).

[21] H. Kamano, S. X. Nakamura, T.-S. H. Lee, and T. Sato, Phys. Rev. C **90**, 065204 (2014).

[22] A. M. Sandorfi, S. Holbit, H. Kamano, and T.-S. H. Lee, J. Phys. G **38**, 053001 (2011).

[23] N. Suzuki, T. Sato, and T.-S. H. Lee, Phys. Rev. C **79**, 025205 (2009).

[24] N. Suzuki, B. Julia-Diaz, H. Kamano, T.-S. H. Lee, A. Matsuyama, and T. Sato, Phys. Rev. Lett. **104**, 042302 (2010).

[25] H. Kamano, S. X. Nakamura, T.-S. H. Lee, and T. Sato, Phys. Rev. C **92**, 025205 (2015).

[26] R. L. Workman, L. Tiator, and A. Sarantsev, Phys. Rev. C **87**, 068201 (2013).

[27] R. A. Arndt, J. M. Ford, and L. D. Roper, Phys. Rev. D **32**, 1085 (1985); R. A. Arndt, W. J. Briscoe, I. I. Strakovsky, and R. L. Workman, Phys. Rev. C **74**, 045205 (2006), and references therein; CNS Data Analysis Center, George Washington University University, http://gwdac.phys.gwu.edu.

[28] See Supplemental Material at http://link.aps.org/supplemental/10.1103/PhysRevC.94.015201 for the values for the model parameters determined by the analysis performed in this work.

[29] W. J. Briscoe, A. E. Kudryavtsev, P. Pedroni, I. I. Strakovsky, V. E. Tarasov, and R. L. Workman, Phys. Rev. C **86**, 065207 (2012).

[30] T. Fujii *et al.*, Phys. Rev. Lett. **26**, 1672 (1971).

[31] Aachen-Bonn-Hamburg-Heidelberg-München Collaboration, P. Benz *et al.*, Nucl. Phys. B **65**, 158 (1973).

[32] T. Fujii *et al.*, Nucl. Phys. B **120**, 395 (1977).

[33] J.-J. Wu, T. Sato, and T.-S. H. Lee, Phys. Rev. C **91**, 035203 (2015).

[34] R. G. Moorhouse, Phys. Rev. Lett. **16**, 772 (1966).

[35] I. G. Aznauryan and V. D. Burkert, Phys. Rev. C **92**, 015203 (2015).

[36] K. A. Olive *et al.* (Particle Data Group), Chin. Phys. C **38**, 090001 (2014).

[37] R. de la Madrid and M. Gadella, Am. J. Phys. **70**, 626 (2002); Nucl. Phys. A **812**, 13 (2008), and references therein.

[38] E. M. Darwish, H. Arenhövel, and M. Schwamb, Eur. Phys. J. A **16**, 111 (2003).

[39] A. Fix and H. Arenhövel, Phys. Rev. C **72**, 064005 (2005).

[40] M. I. Levchuk, A. Yu. Loginov, A. A. Sidorov, V. N. Stibunov, and M. Schumacher, Phys. Rev. C **74**, 014004 (2006).

[41] M. Schwamb, Phys. Rep. **485**, 109 (2010).